Materials Horizons

ROYAL SOCIETY OF CHEMISTRY

COMMUNICATION

View Article Online
View Journal

Cite this: DOI: 10.1039/d1mh00521a

Received 29th March 2021,
Accepted 7th May 2021

DOI: 10.1039/d1mh00521a

rsc.li/materials-horizons

Metallic glue for designing composite materials with tailorable properties†

Jianan Fu,[a] Jian Yang,[a] Kai Wu,[a] Hongji Lin,[a] Wenxin Wen,[a] Wenqing Ruan,[a] Shuai Ren,[a] Zhenxuan Zhang,[a] Xiong Liang[a] and Jiang Ma *[ab]

Developing materials with tailorable properties has been the long-sought goal of humankind. Forming composite materials with superior properties by combining two or more materials has emerged as a competitive means in the search and design of new materials. However, it is still a grand challenge to use metallic materials as a binder for composites because of their lack of adhesion. In the present work, we proposed a facile and flexible route to synthesize composites using metallic glass as a glue to bond various materials, ranging from conductors to insulators, and metals to nonmetals, together. The mechanical, magnetic and electrical performances of the composites can be manually regulated by changing the addition ratios of the metallic glass glue and the corresponding admixture. In addition, porous structures were also obtained and tuned by dissolving the soluble admixture in water. In principle, our approach provides a new idea for the fabrication and optimization of composites using metallic materials as binders. The outcome of our current research opens up a window not only to synthesize composite materials with tailorable properties universally and flexibly, but also towards the discovery of potential multi-functional metal containing composites.

New concepts

To design materials with desirable and tailorable properties is a long standing goal and of significant general interest to the material science community. In this work, we propose a new concept to design and synthesize composites using metallic materials as binders. Benefiting from the thermoplastic forming ability of metallic glass (MG), various materials, ranging from conductors to insulators and metals to non-metals, could be bonded together with MG firmly and densely in a facile and flexible way. The mechanical, magnetic and electrical performances of the composites can be manually regulated by changing the addition ratios of the MG binder and admixtures. In addition, porous structures were also obtained and tuned by dissolving the soluble admixture in water, and the pore size can be regulated according to the particle size of the water soluble admixture. The outcome of the current research opens up a window not only to design composite materials universally and flexibly, but also towards the discovery of potential multi-functional composites. This could be a totally new concept for the development of superior materials, and inspire a new wave of research, such as searching for more MG systems as binders, trying multi-binders with several different MG compositions together and so on.

Introduction

Materials have such an influence on our lives that the historical periods of humankind have been dominated and named after materials, known as the Stone Age, Bronze Age, Iron Age and Silicon Age we are now in.[1] The field of materials is immense and diverse with various properties, and the demand for materials is endlessly growing. Therefore, the pressure on the development of new materials is becoming formidable. For most of recorded history, the control of materials has been through alchemy or empirical means to develop materials with desirable properties. Nowadays, one effective strategy to fabricate composite materials with a tailorable specific property is to combine two or more materials to achieve properties that are superior to those of each constituent.[2–5] Composite materials with structures combining two or more of the basic types of materials, perhaps, have the most incredible future of all.[6,7]

As the oldest natural composites, wood that consists of cellulose fibers in a lignin matrix[8] and bone that consists of fibers embedded in an interstitial bone matrix[9] inspire us to develop new materials. Dating back to the use of straw-reinforced clay for buildings, man-made composites find extensive prospects both in scientific research and engineering applications.[10] For example, rocks are combined with cement to make concrete[11] and polyester resin reinforced with glass fibers to manufacture a firm boat.[12] Therefore, designing and fabricating composites that satisfy needs have been playing

[a] College of Mechatronics and Control Engineering, Shenzhen University, Shenzhen 518060, China. E-mail: majiang@szu.edu.cn
[b] Shenzhen Key Laboratory of High Performance Nontraditional Manufacturing, College of Mechatronics and Control Engineering, Shenzhen University, Shenzhen, 518060, China

† Electronic supplementary information (ESI) available. See DOI: 10.1039/d1mh00521a

significant roles in extensive engineering applications, and even the development of society.

Composites involve several concerns, including the ability to bind different materials together, the efficient stress distribution across a joint, the cost-effectiveness of an easily mechanized process, and greater flexibility in design. Based on the above considerations, thermoset or thermoplastic polymer materials combining with reinforced fibers are a common strategy to produce composites.[2,13–15] However, metals that have excellent mechanical performances are seldom used as the binder for composites because of their lack of adhesion. It is believed that metals mixed with other materials in a controlled way to form composites with an outstanding combination of properties could bring developments in different material families that may thus benefit from each other.[16] Thus, to develop and tailor composites with metallic binders would be of great significance.

In the present work, we propose a facile and flexible method to synthesize composites using metallic glass (MG), which has superior properties,[17–21] as the glue. Benefiting from the thermoplastic forming ability of MG,[22–26] various materials, ranging from conductors to insulators and metals to nonmetals, could be bonded together with the MG firmly and densely in a very straightforward way. The mechanical, magnetic and electrical performances of the composites can be manually regulated by changing the addition ratios of the MG glue and the admixture. In addition, porous structures were also obtained and tuned by dissolving the soluble admixture in water. The results show that the proposed concept is an effective method to fabricate composites with tailorable properties, such as mechanical, magnetic and electrical properties when compared with previous literature.[27–35] It also provides a new and universal strategy to fabricate composites with tailorable properties, meanwhile throwing light on the discovery of potential multi-functional metal containing composites.

Experimental methods

Preparation of the MG and admixture particles

The MG used in this work was La-based MG $La_{55}Al_{25}Ni_5Cu_{10}Co_5$ (at%) because of its wide supercooled liquid region (SLR) and fine thermoplastic forming ability at moderate temperatures.[36–38] The $La_{55}Al_{25}Ni_5Cu_{10}Co_5$ ribbons were prepared by a conventional melt spinning process. The amorphous ribbons were cut into small particles with the size ranging from 150 μm to 200 μm. Then, they were uniformly mixed together with the admixture particles ($<$200 μm) by stirring and shaking repeatedly. The mass ratios of CoCrFeNiMn high entropy alloy (HEA) powders, Cordierite ceramic powders and Fe-based MG ($Fe_{78}Si_9B_{13}$) powders over the MG were varied with 8 : 2, 6 : 4, 5 : 5, 4 : 6, and 2 : 8 (wt%), respectively. The mixture ratio of the other powders over the MG was 5 : 5 (wt%).

Bonding process

When the temperature raised to the SLR of the La-based MG (around 500 K) in a vacuum chamber, a pressure of 460 MPa was applied to the specimen at a rate of 0.05 mm s^{-1} and maintained for about one minute. After this, the pressure was unloaded to 0 MPa quickly, and the specimen was taken out of the chamber.

Multi-scale structural characterizations

X-ray diffraction (XRD; RIGAKU miniflex600) with Cu Kα radiation was used to detect La-based MG powders, and admixtures and their composites were obtained by hot bonding. Differential scanning calorimetry (DSC; PerkinElmer DSC-8000) at a heating rate of 20 K min^{-1} was used to detect La-based MG powders. The scanning electron microscope (SEM; Fei quanta FEG 450) instrument equipped with energy disperse spectroscopy (EDS) was used to observe the micro morphology and elemental distribution of the composites. The atomic structure was characterized using JEM-2100F transmission electron microscopy (TEM) with EDS. The TEM samples were prepared on a FEI Scios SEM/FIB dual beam system. According to the ASTM standard,[39] the cylinder specimens with a length/diameter ratio of 1.5 (length 4.5 mm and diameter 3 mm) were compressed with Z050TEW (strain rate 0.001 s^{-1}) at room temperature. Both ends of the specimens were polished parallel with each other before the mechanical test. The magnetic hysteresis loops were obtained at room temperature by a magnetic property measurement system (MPMS3) to test the magnetic properties of the composites. The resistance of the specimens was tested by a digital multimeter (Tektronix DMM 4020 5-1/2) combined with Kelvin Four-terminal sensing, and the specimens were measured five times to ensure that the data were reliable. The densities of the obtained composites were tested on a density balance following the buoyancy principle. An electronic balance (Sartorius Quintix35-1CN, measurement accuracy 0.01 mg) was used to measure the weight of the composites by hot bonding.

Results and discussion

Bonding various materials with the MG

Fig. 1a schematically describes the bonding and combination of the MG and admixture powders during heating and pressing. Based on this simple and convenient combination method, the MG can be used as the glue to bond various kinds of materials. Fig. 1b–e and j–m present the SEM images of HEA, ceramic, Fe-based MG, glass (SiO_2), cement, sand, alloy and NaCl particles after bonding with the MG, and their photos are also shown in each inset. The photographic figure of the composite block and the SEM images of the internal bonding of this composite block provide evidence for the integrity and firmness of the composites, and their corresponding XRD patterns are displayed in Fig. 1f–i and n–q. A typical amorphous peak and characteristic peaks can be found in the XRD patterns for the MG and admixture feedstocks. However, when the MG and admixture were bonded to form bulk composites, both the amorphous peak and the sharp characteristic peaks appeared in the XRD patterns, indicating that two phases were mixed together in the composites. The glass transition temperature (T_g) and the

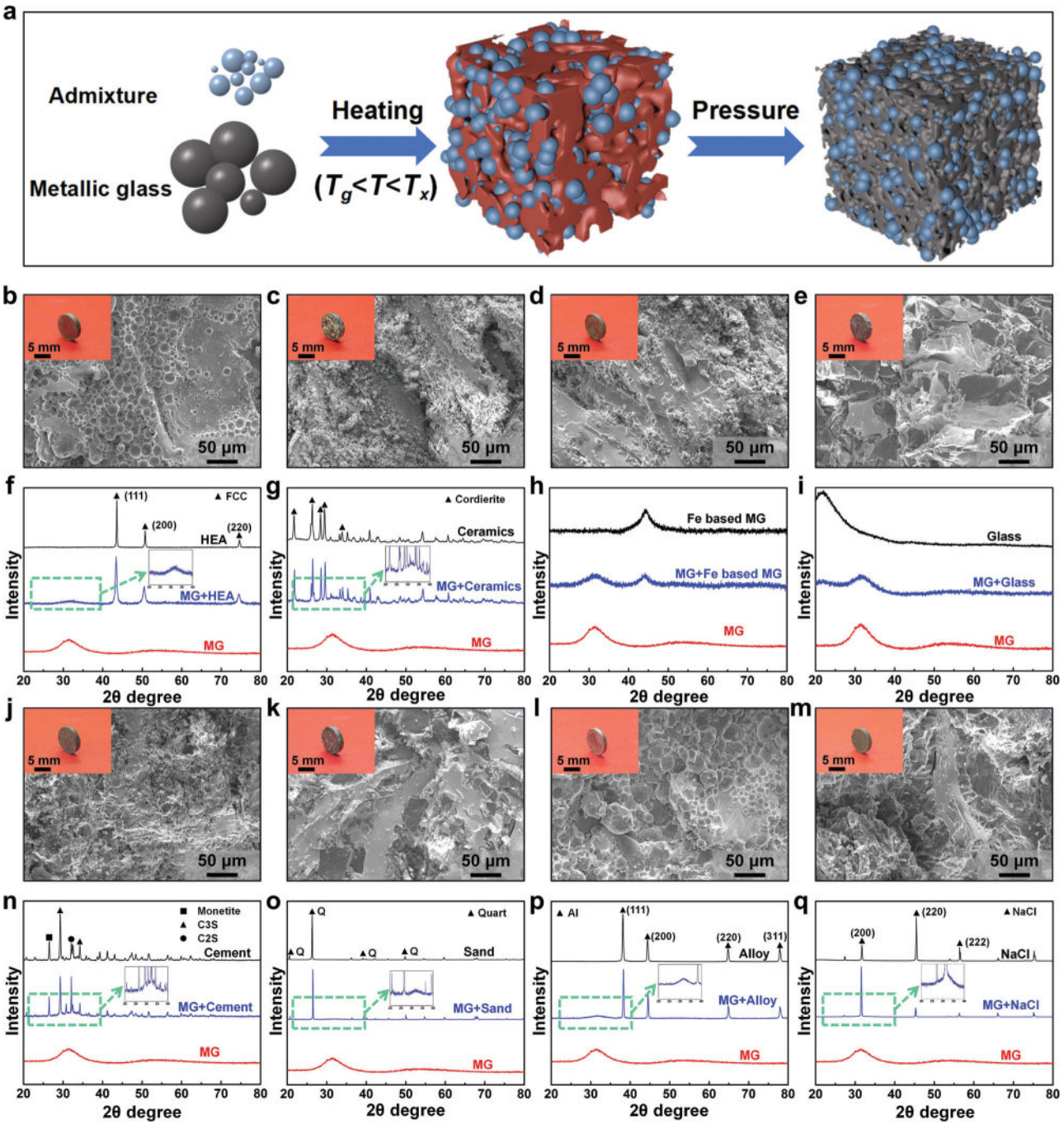

Fig. 1 Bonding various materials with the MG. (a) A schematic diagram of the MG bonding the admixture. (b–e) The internal SEM images of the composites formed by the MG combined with HEA, ceramic, Fe-based MG and glass with their photos in each inset. (f–i) The XRD patterns of the composites of HEA, ceramic, Fe-based MG and glass with the MG. (j–m) The internal SEM images of the composites formed by the MG combined with cement, sand, alloy and NaCl with their photos in each inset. (n–q) The XRD patterns of the composites of cement, sand, alloy and NaCl with the MG.

crystallization temperature (T_x) of La-based MG were measured to be 456 K and 514 K, respectively, by DSC (see Fig. S1, ESI†). It can be seen that the broad SLR (58 K) facilitates hot bonding. The results above show that the MG can be used as the glue to bond a variety of materials, ranging from conductors to insulators and metals to nonmetals, and the bonding quality is quite good. This could be a flexible strategy to manually design materials with desirable performances.

Bonding mechanisms

To further investigate the bonding mechanisms of the composites, TEM is applied to characterize the interface of the composite between MG and HEA. Fig. 2a shows the SEM image of the MG glue bonding HEA, and it can be clearly seen that there is no crack in the bonding area. The low-resolution TEM image of the interface between the MG glue and HEA is shown in Fig. 2b; this further reveals the excellent combination

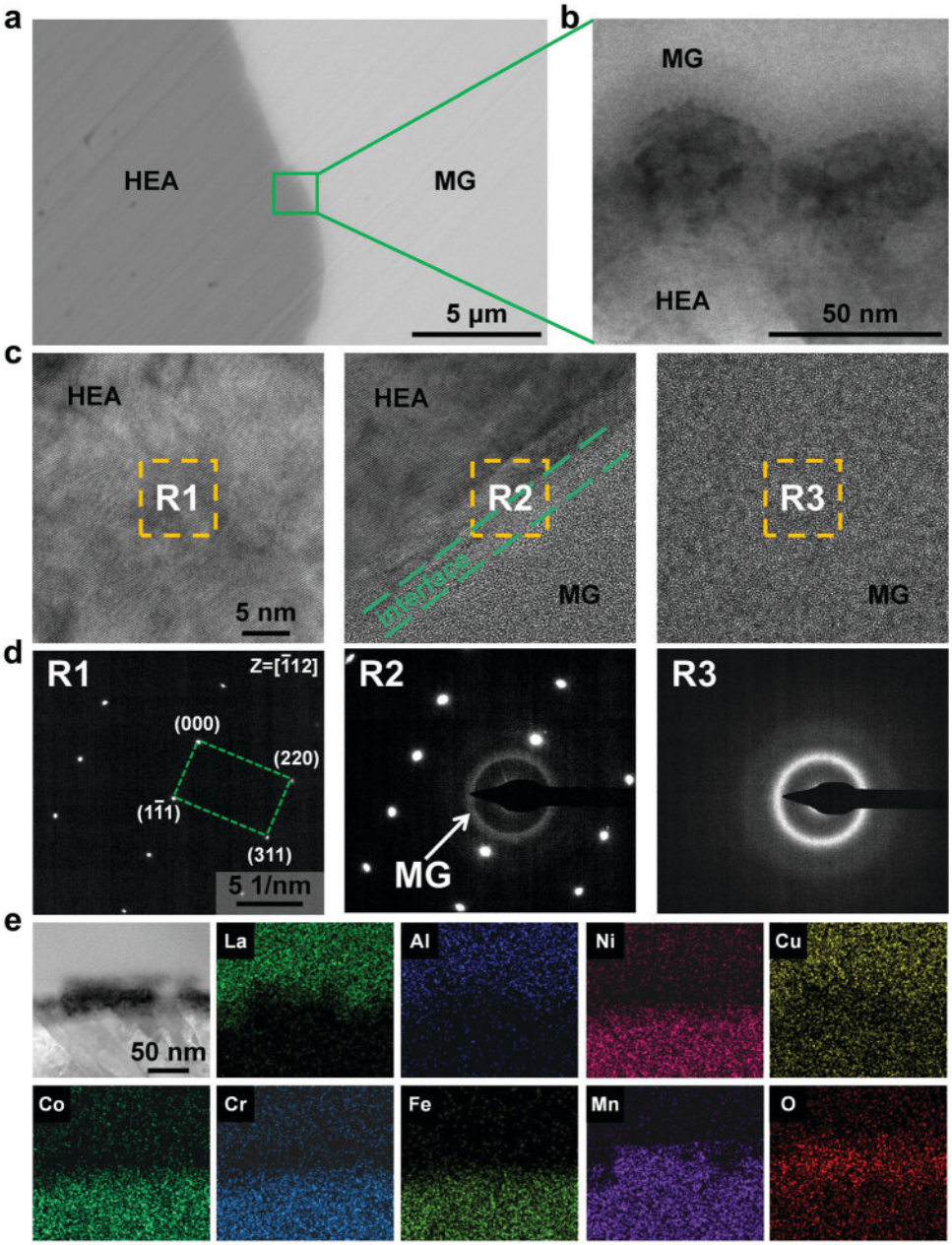

Fig. 2 TEM characterization of the composite. (a) The SEM image of the composite between MG and HEA. (b) The TEM image of the composite between MG and HEA. (c) The high-resolution TEM image of the composite in the HEA region, interface region and MG region. (d) The diffraction patterns of the regions R1, R2 and R3. (e) The elemental distribution of the composite at the interface.

between MG and HEA. The corresponding high-resolution TEM images in the HEA region, interface region and MG region are displayed in Fig. 2c. It can be found that MG and HEA show completely distinct structures under the observation of a high-resolution transmission electron microscope (HRTEM). The MG region is typical amorphous structures, while the HEA region is typical crystal structures. When HRTEM is used to observe the region with an interface, it can be seen that the atoms on one side of the interface are ordered, while the atoms on the other side are disordered. Three regions R1, R2 and R3 are selected from the high-resolution TEM images for the selected area electron diffraction (SAED), and the results are presented in Fig. 2d. The diffraction spots in the R1 region show the crystalline state, which corresponds to HEA. For R2 with the interface region, the diffraction pattern shows the combination of diffraction spots and a halo ring. When the region moves to R3, the diffraction spots disappear completely and the diffraction pattern only exhibits a halo ring, which is consistent with the XRD results. The crack of an oxide layer is very crucial for the MG glue to bond various admixtures;[40–42] thus it is necessary to overcome the oxide barrier during hot bonding. Fig. 2e summarizes the image of low-resolution TEM

and the corresponding surface scan energy spectrum at the interface during hot bonding. The image of low-resolution TEM clearly reveals that the MG bonds tightly to HEA like a glue. The energy spectrum shows the elemental distribution of MG and HEA at the interface. To specifically compare the change of oxygen element distribution at the combination and non-combination, the line scan energy spectrum is applied (see Fig. S2, ESI†). When lines 1 and 3 are used to scan at the combination, the change of an oxygen element had no obvious fluctuation. In contrast, a sudden change of the oxygen content occurs in the middle part of the line 2, which is caused by the oxide layer. The existence of the oxide layer hinders the combination, corresponding to the observed results. It reveals that the MG as the glue to the admixture is a kind of combination to break through the oxide layer and forms excellent bonding.

Mechanical performance regulation

To verify the performance modulation ability using such a strategy, we try to design materials with tailorable mechanical, magnetic, electrical and porous properties by changing the ratios of the MG and admixture. Firstly, the materials with excellent comprehensive mechanical performances were obtained by bonding HEA using the MG glue. CoCrFeNiMn (HEA) has superior ductility, however poor strength.[43] To address this issue, the high strength MG could be used as the glue to bond HEA together to achieve better comprehensive mechanical performance by adjusting the addition ratios of HEA and MG.[44] Fig. 3a shows the XRD patterns of MG and HEA mixed with five different mass fraction ratios 2 : 8, 4 : 6, 5 : 5, 6 : 4, and 8 : 2, and the XRD patterns of MG and HEA are also included. It can be seen that the pure HEA has characteristic crystalline peaks and the MG has a typical amorphous peak at

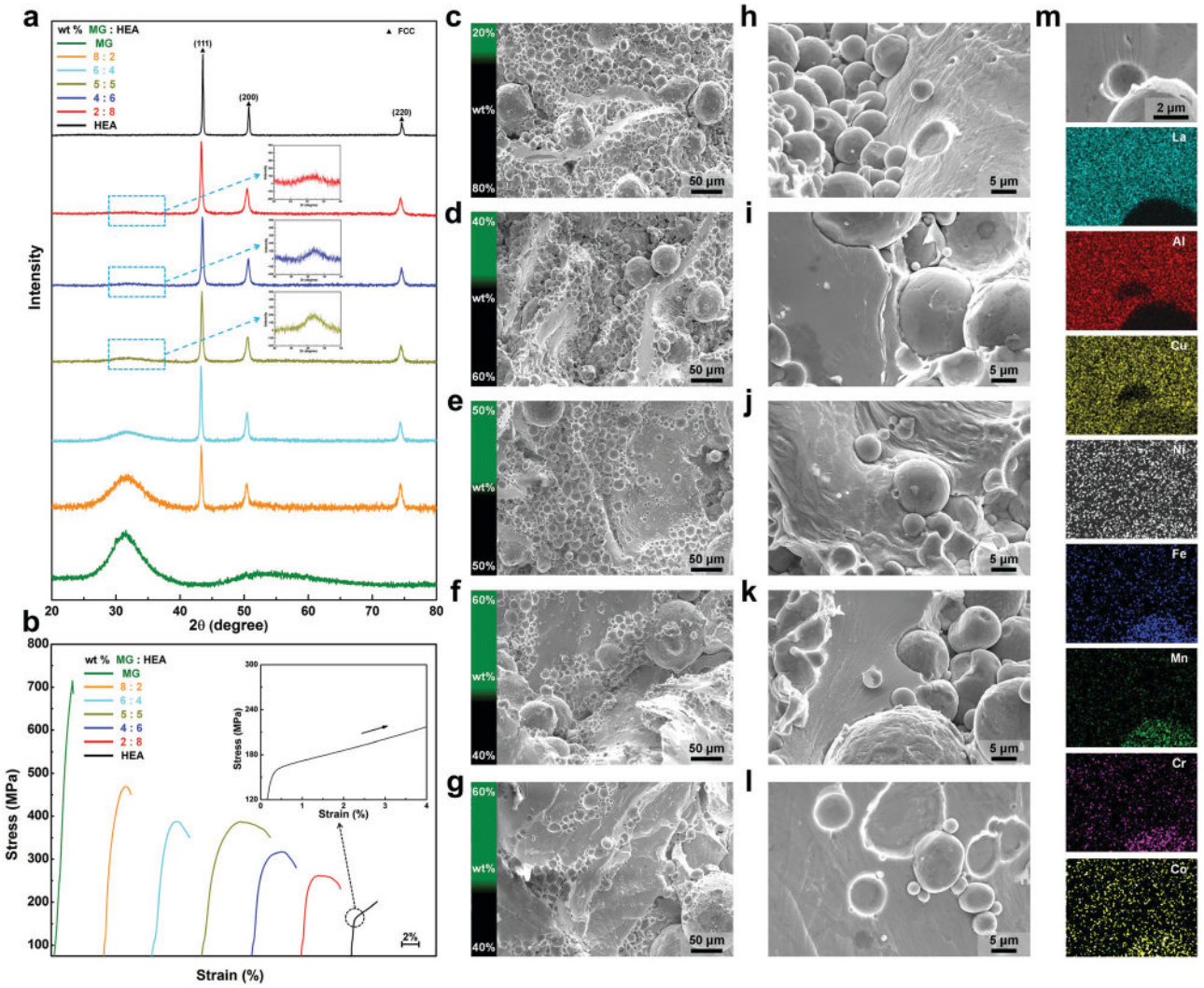

Fig. 3 Mechanical performance regulation. (a) The XRD patterns of MG, HEA and the composites formed by HEA and MG at different ratios. (b) The mechanical properties of MG, HEA and the composites formed by HEA and MG at different ratios. (c–g) The SEM images of the MG bonded with HEA in the ratios of 2 : 8, 4 : 6, 5 : 5, 6 : 4, and 8 : 2 (wt%) at low magnification. (h–l) The SEM images of the MG combined with HEA in the ratios of 2 : 8, 4 : 6, 5 : 5, 6 : 4, and 8 : 2 (wt%) at high magnification. (m) The elemental distribution in a micro-region that contains both the MG and HEA.

about 32°. With the increasing ratio of MG, the amorphous peak gradually becomes steeper and steeper for the composites.

The bonding quality of MG and HEA was deeply explored by SEM observation and density measurement. During the experiment, the actual densities of the composites can be calculated by the formula $\rho_{actual} = (w_1 \cdot \rho_1)/(w_1 - w_1)$, where ρ_{actual} denotes the actual densities of the composites, w_1 is the weight of the composites in air, w_2 represents the weight of the composites in distilled water, and ρ_1 is the density of the distilled water (0.999 g cm^{-3}) at room temperature. The densities of the composites with different mass ratios were tested by the buoyancy principle. The theoretical densities of the composites can be calculated according to their mixture ratios by the following eqn (1):

$$\rho_{composite} = \frac{(w_{MG} + w_{admixture})}{(w_{MG}/\rho_{MG} + w_{admixture}/\rho_{admixture})} \quad (1)$$

In eqn (1), $\rho_{composite}$ denotes the theoretical densities of the composites, w_{MG} represents the weight of La-based MG, $w_{admixture}$ is the weight of admixture, ρ_{MG} represents the density of La-based MG, and $\rho_{admixture}$ represents the densities of the admixture.

The maximum error between the actual density and the theoretical density (see Fig. S3, ESI†) is only 2%, indicating that the bonding is very intact and solid. In addition, as shown in Fig. 3a–g (from top to bottom, MG : HEA (wt%) is 2 : 8, 4 : 6, 5 : 5, 6 : 4, and 8 : 2), the micro morphology of MG combined with HEA is described under a magnification level of 1000×. Fig. 3h–l shows the detailed SEM images of the combination of MG and HEA under a magnification level of 8000×. It can be clearly seen that the MG flows and acts as the glue to join HEA tightly during the bonding process. The SEM images and densities of the composite present solid evidence that the inner part of the composites is dense. The elemental distribution of MG and HEA after bonding is presented in Fig. 2m, which is consistent with the elements contained in the materials used in the experiment.

The stress–strain curves under compression at room temperature of the as-fabricated composites with different mass ratios are shown in Fig. 3b. The stress–strain compression curves of the pure MG and HEA under the same conditions are also displayed as a comparison. It can be seen that the La-based MG shows a large compressive strength of 714 MPa, but a very poor plasticity. Although the yield strength of HEA is only 161 MPa, it shows excellent compression plasticity. The tendency of the mechanical performance is very obvious when the two materials are bonded together with different ratios. The composites have the advantages of the two materials at the same time, and the strength and plasticity of the composites show a certain rule with the change of the ratio. The specific mechanical values such as strength and strain are shown (ESI† Table S1).

It can be found from Fig. 3b that the compressive strength of the composites increases with the increasing proportion of the La-based MG in the ratios. For strain, compared with the pure La-based MG, the strain of the composites also has a certain increasing rule, and the maximum strain of 8% is reached when the ratio is 5 : 5 (wt%). The mechanical performance of the composites shows that the bonding of HEA using the MG as the glue provides a potential method to regulate new materials with better comprehensive performances.

Magnetic performance regulation

The functional magnetic performance of the composites can also be regulated by bonding the Fe-based MG with the MG glue. Following the same bonding process, La-based MG and Fe-based MG are homogeneously mixed by five different ratios (La-based MG : Fe-based MG (wt%) is 2 : 8, 4 : 6, 5 : 5, 6 : 4, and 8 : 2), and their composites are obtained.

The intrinsic structure of the composites as well as the pure MG glue and Fe-based MG is characterized by XRD and is displayed in Fig. 4a. It can be clearly seen that there are typical amorphous peaks in the XRD patterns of the MG glue and Fe-based MG. The two amorphous phases of La-based MG and Fe-based MG are found in their composites. And with the increasing proportion of La-based MG in the proportion, the corresponding amorphous peak value of La-based MG will gradually rise. Meanwhile, the amorphous peaks value corresponding to the Fe-based MG will be weaker.

The internal micrographs of the composites are shown in Fig. 4c–g. A mass fraction ratio strip is placed on the left side of each SEM image to better distinguish the differences between the composites. It can be seen from the figures that the content of the MG glue and Fe-based MG in the composites is very obvious with the change of ratios. The SEM images presented in Fig. 4h–l show more details of the bonding. It can be found that the small particles of Fe-based MG are tightly bonded to the MG glue, and no holes are observed. Meanwhile, the maximum error between actual density and theoretical density is only 2.4% (see Fig. S4, ESI†), which corresponds to the SEM observation. The elemental analysis maps are shown in Fig. 3m, where the La-rich region is the MG glue (La-based MG) while the Fe-rich region is the Fe-based MG.

After the introduction of magnetic Fe-based MG into the composites, the hysteresis loops were tested to analyze its magnetic behavior at room temperature. The hysteresis loops of the MG glue, Fe-based MG and their composites at different ratios are shown Fig. 4b. It can be seen that the magnetic properties of Fe-based MG and La-based MG are extremely different. The saturation magnetization (M_s) value of Fe-based MG is 145.19 emu g^{-1}, while that of La-based MG is nearly 0 emu g^{-1}. In addition, the hysteresis loops of the composites also show a large gap. When the ratio of Fe-based MG in the composites changes from 20% to 80% wt, the corresponding M_s values of the composites are 109.20 emu g^{-1}, 87.65 emu g^{-1}, 71.17 emu g^{-1}, 50.00 emu g^{-1} and 32.54 emu g^{-1}, respectively. The composite of 80% wt Fe-based MG and 20% wt MG glue shows the largest M_s value. This is consistent with the largest proportion of Fe-based MG. The other composites also show an obvious tendency, with the decrease of the proportion of Fe-based MG in the composites, the corresponding M_s value also gradually decreases. The hysteresis loops of the composites

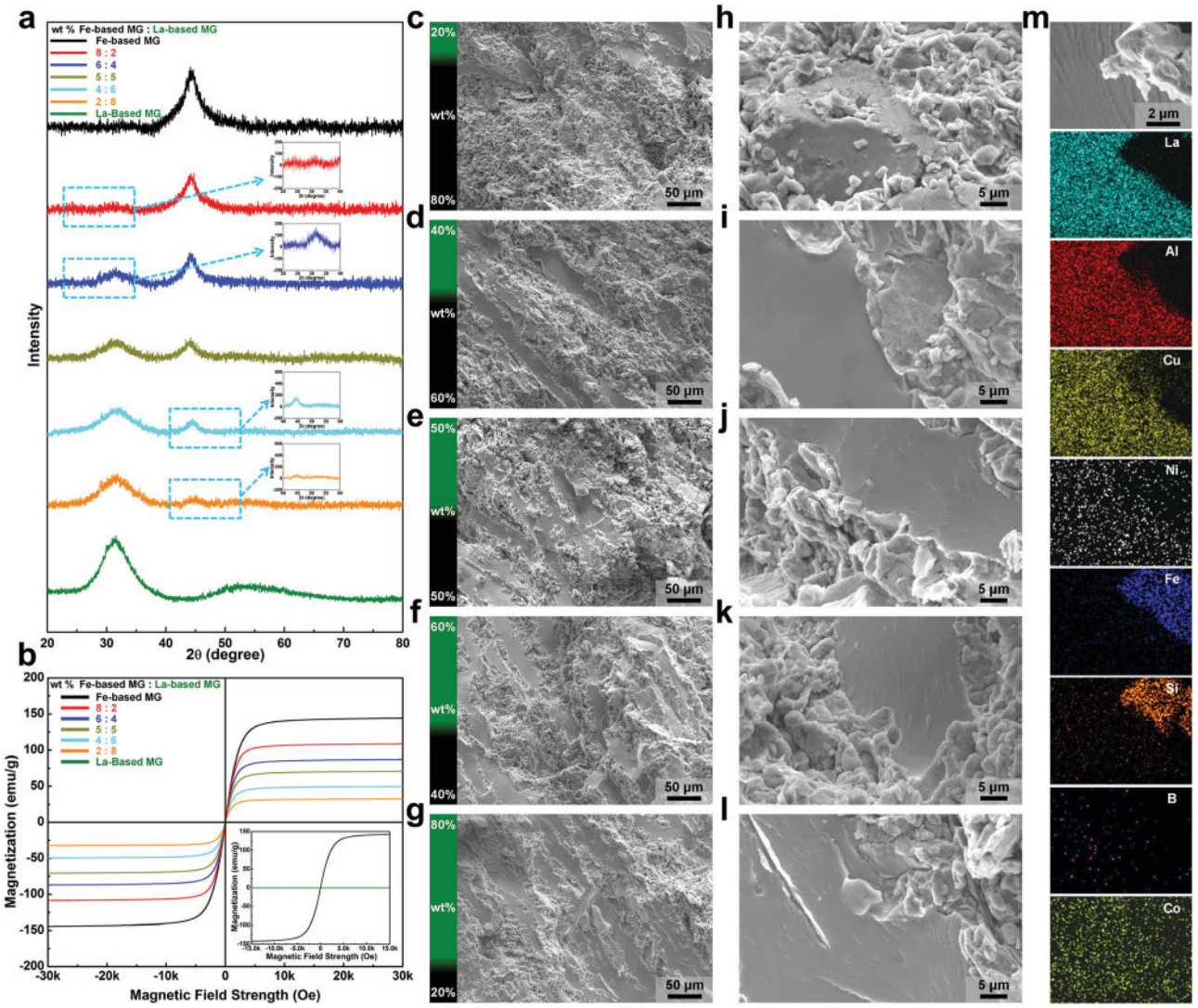

Fig. 4 Magnetic performance regulation. (a) The XRD patterns of La-based MG, Fe-based MG and the composites formed by La-based MG and Fe-based MG at different ratios. (b) The magnetic properties of La-based MG, Fe-based MG and the composites formed by La-based MG and Fe-based MG at different ratios. (c–g) The internal SEM images of La-based MG combined with Fe-based MG in the ratios of 2 : 8, 4 : 6, 5 : 5, 6 : 4, and 8 : 2 (wt%) at low magnification. (h–l) The internal SEM images of La-based MG combined with Fe-based MG in the ratios of 2 : 8, 4 : 6, 5 : 5, 6 : 4, and 8 : 2 (wt%) at high magnification. (m) The elemental distribution in a micro-region that contains both the La-Based MG and Fe-based MG.

indicate that the magnetic properties of the composites can be precisely regulated by changing the ratio of the MG glue and Fe-based MG to obtain any desirable magnetic properties.

Electrical performance regulation

Based on the above combination method, we also used the MG glue to bond insulator (ceramics) to regulate its electrical properties. The mass fraction ratios of the MG glue and ceramics in the composite are 8 : 2, 6 : 4, 5 : 5, 4 : 6, and 8 : 2, respectively. The XRD patterns of the composites and the raw materials before their combination are shown in Fig. 5a. It can be seen that the XRD patterns of the ceramics have many characteristic peaks, and the whole pattern is very flat. The XRD patterns of the composites also show the same characteristic peak as that of the ceramics, but these patterns are not flat and show a peak at 32°, which is caused by the MG glue in the composites, and the peak value is positively proportional to the MG content in the composites.

The bonding quality is an important standard to evaluate the quality of the composites. To this, the internal images of SEM and the densities of the composites are analyzed. Fig. 5c–g shows five kinds of composite SEM images with different ratios in a large field of vision; it can be found that small particles of ceramics are bonded around the MG, and Fig. 5h–l reveals the bonding part between the MG glue and ceramics in a smaller area, which means that the interior of the composites is compact. The densities of the composites are summarized (see Fig. S5, ESI†). The maximum error of the densities of the composites measured by buoyancy is only 3%, which further proves that the inner part of the composites is dense. Fig. 4m displays the energy spectrum of a micro-region, which contains both ceramics and MG. The element types obtained from the

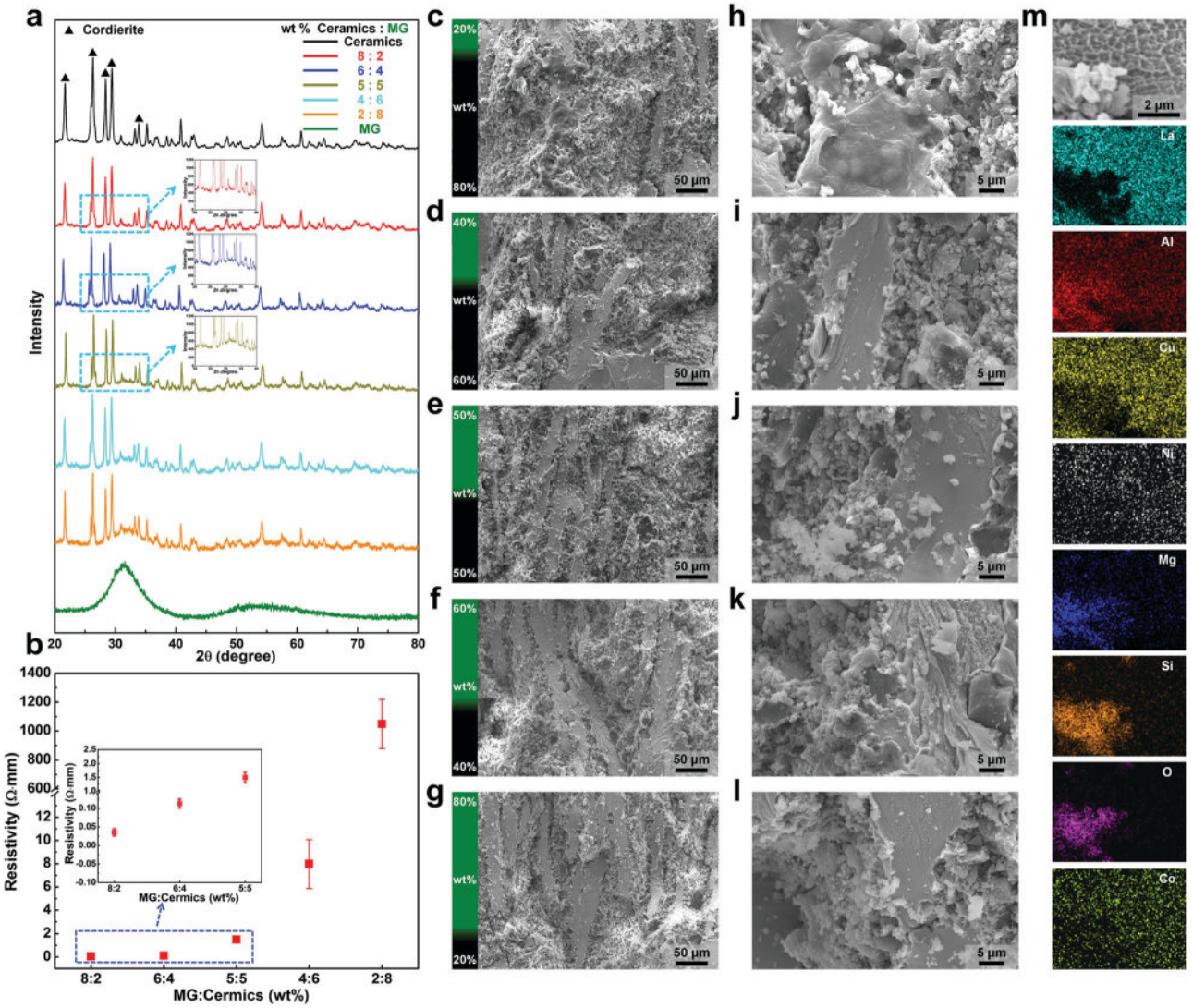

Fig. 5 Electrical properties regulation. (a) The XRD patterns of MG, ceramics and the composites formed by MG and ceramics at different ratios. (b) The electrical properties of MG, ceramics and the composites formed by MG and ceramics at different ratios. (c–g) The internal SEM images of MG combined with ceramics in the ratios of 2 : 8, 4 : 6, 5 : 5, 6 : 4, and 8 : 2 (wt%) at low magnification. (h–l) The internal SEM images of MG combined with ceramics in the ratios of 2 : 8, 4 : 6, 5 : 5, 6 : 4, and 8 : 2 (wt%) at high magnification. (m) The elemental distribution in a micro-region that contains both the MG and ceramics.

energy spectrum analysis are the same as those of the materials used in the experiment.

The resistance of the composites with different ratios was tested. To compare the difference of conductivity between each specimen, the resistivity of each specimen is calculated by $\rho_{\text{resistivity}} = R{\cdot}S/L$, where $\rho_{\text{resistivity}}$ denotes the resistivity of the composites, R represents the resistance of the composites at room temperature, S and L separately represent the cross-sectional area and the length of the composites. After using the above formula, the resistivities of the composites with different ratios are displayed in Fig. 5b. It can be found that with the ratio of ceramics increasing in the composites, the resistivity of the composite (MG : ceramics is 8 : 2 wt%), composite (MG : ceramics is 6 : 4 wt%), and composite (MG : ceramics is 5 : 5 wt%) increases linearly. However, when the ratios of the ceramics continue to increase, a sharp increase in resistivity is observed, and the maximum resistivity could reach 1048.41 Ω mm when the ceramics increased to 80% wt of the total. This does not affect the rule that the resistivities increase with the increasing ratios of ceramics in the composites. This also means that we use the MG as the glue to prepare a new material that can adjust its conductivity.

Porous structure regulation

Amazingly, the densification of materials can be manipulated; therefore, porous materials are obtained by using the MG as the glue. As presented in Fig. 6a, after the combination of MG and soluble NaCl particles, the bonded blocks were placed in distilled water for 10 minutes to dissolve the NaCl particles (see Movie S1, ESI†). After the dissolution of NaCl particles, the porous structures were obtained on the blocks. To assess the intrinsic structure of the blocks before and after dissolution,

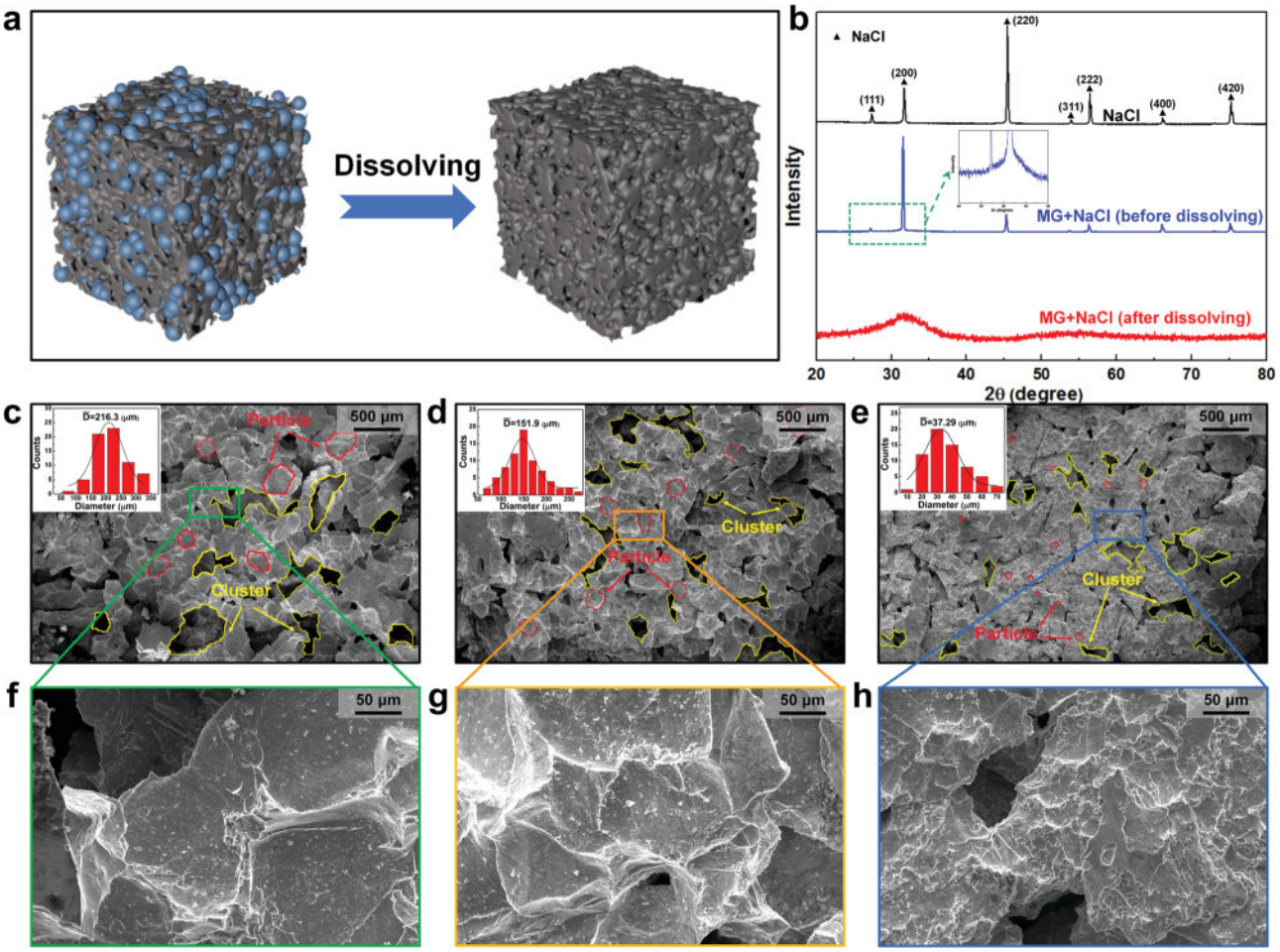

Fig. 6 Porous structure regulation. (a) A schematic diagram of NaCl in the dissolved composite. (b) The XRD patterns of NaCl, the composite of NaCl and MG, and the composite after dissolving NaCl. (c–e) The SEM images of the composites after dissolving NaCl with particle sizes of 200 μm, 125 μm, and 48 μm at low magnification. (f–h) The SEM images of the composites after dissolving NaCl with particle sizes of 200 μm, 125 μm, and 48 μm at high magnification.

the results (see Fig. 6b) obtained by XRD clearly show that the blocks before dissolving include both amorphous phase and NaCl characteristic peaks. When the blocks are dissolved, it remains amorphous without any crystallization peaks, which further proves that the NaCl in the block has been completely removed. After dissolving NaCl, the surface morphology was observed by SEM at high and low magnifications. Fig. 6c–e clearly reveals the SEM images of the MG glue combined with NaCl with particle sizes of 200 μm, 125 μm, and 48 μm at low magnification, and the SEM images with high magnification (Fig. 6f–h) correspond to the lower part, respectively. In the upper left corner inset, we calculated the particle size distribution of each specimen, the average particle size obtained is 216.3 μm, 151.9 μm, and 37.29 μm, corresponding to the size of the NaCl particles that were used. Additionally, we can see that there are many large holes on the surface of the specimen, which are caused by the gathering of the NaCl particle clusters. Some pits can be observed in the high magnification SEM images, which are caused by a single NaCl particle. It can be seen that we can easily prepare porous materials and can also adjust the size of the internal structure by adjusting the size of the admixture.

Conclusion

In summary, we successfully use MG as the glue to bond all kinds of materials and the mechanisms of bonding are also investigated. Adjusting the ratios of MG to HEA, ceramics and Fe-based MG, the desirable mechanical, electrical and magnetic properties can be obtained. In addition, porous structures are also obtained and tuned by dissolving the soluble admixture in water. This method developed in the paper provides great potential for the composites with tailorable properties and offers instructive inspirations for the multi-component composites. The composites with tailorable properties such as mechanical properties, magnetic properties, electrical properties and the porous structure will also have potential applications in automobile, heater, microwave components, catalysis, *etc.*

Data and material availability

All data needed to evaluate the conclusions in the paper are present in the paper and/or the ESI† Materials. Additional data related to this paper may be requested from the authors.

Author contributions

Jianan Fu and Jiang Ma conceived the idea. Jiang Ma, Wenqing Ruan, Shuai Ren, Zhenxuan Zhang and Xiong Liang supervised the work. Jianan Fu and Hongji Lin carried out the thermo bonding experiments and Jian Yang designed and completed the experimental setup. Wenxin Wen performed XRD, DSC and TEM. Jianan Fu and Jiang Ma wrote the manuscript. All authors contributed to the discussion and analysis of the results.

Conflicts of interest

The authors declare no competing financial interest.

Acknowledgements

The work was supported by the Key Basic and Applied Research Program of Guangdong Province, China (Grant Nr. 2019B030302010), the NSF of China (Grant Nr 51871157 and 51971150), the Science and Technology Innovation Commission Shenzhen (Grants No. JCYJ20170412111216258), and the National Key Research and Development Program of China (Grant No. 2018YFA0703604). The authors also acknowledge the assistance on the microscopic observation received from the Electron Microscope Center of the Shenzhen University.

References

1 W. D. Callister, *Materials science and engineering an introduction*, John Wiley, 2007.
2 E. J. Barbero, *Introduction to composite materials design*, CRC press, 2017.
3 J. Ma, C. Yang, X. Liu, B. Shang, Q. He, F. Li, T. Wang, D. Wei, X. Liang and X. Wu, *Sci. Adv.*, 2019, **5**, eaax7256.
4 X. Liang, X. Zhu, X. Li, R. Mo, Y. Liu, K. Wu and J. Ma, *Sci. China: Phys., Mech. Astron.*, 2020, **63**, 116111.
5 T. Saito, Y. Oaki, T. Nishimura, A. Isogai and T. Kato, *Mater. Horiz.*, 2014, **1**, 321–325.
6 K. K. Chawla, *Composite materials: science and engineering*, Springer Science & Business Media, 2012.
7 J. Yang, L. S. Tang, L. Bai, R. Y. Bao, Z. Y. Liu, B. H. Xie, M. B. Yang and W. Yang, *Mater. Horiz.*, 2019, **6**, 250–273.
8 F. W. Jane, *The structure of wood*, 1956.
9 S. Weiner and W. Traub, *FASEB J.*, 1992, **6**, 879–885.
10 C. R. Reddy, A. P. Sardashti and L. C. Simon, *Compos. Sci. Technol.*, 2010, **70**, 1674–1680.
11 P. K. Mehta, *Concrete. Structure, properties and materials*, 1986.
12 T. Sathishkumar, S. Satheeshkumar and J. Naveen, *J. Reinf. Plast. Compos.*, 2014, **33**, 1258–1275.
13 A. D. Valino, J. R. C. Dizon, A. H. Espera Jr, Q. Chen, J. Messman and R. C. Advincula, *Prog. Polym. Sci.*, 2019, **98**, 101162.
14 Z. M. Li, S. N. Li, M. B. Yang and R. Huang, *Carbon*, 2005, **43**, 2413–2416.
15 B. G. Compton, B. K. Post, C. E. Duty, L. Love and V. Kunc, *Addit. Manuf.*, 2017, **17**, 77–86.
16 K. Lu, *Science*, 2010, **328**, 319–320.
17 W. Klement, R. H. Willens and P. Duwez, *Nature*, 1960, **187**, 869–870.
18 W. H. Wang, C. Dong and C. H. Shek, *Mater. Sci. Eng., R*, 2004, **44**, 45–89.
19 Z. P. Lu and C. T. Liu, *Acta Mater.*, 2002, **50**, 3501–3512.
20 A. Inoue, *Acta Mater.*, 2000, **48**, 279–306.
21 Y. Yan, C. Wang, Z. Huang, J. Fu, Z. Lin, X. Zhang, J. Ma and J. Shen, *J. Mater. Chem. A*, 2021, **9**, 5415–5424.
22 J. Ma, X. Zhang, D. Wang, D. Zhao, D. Ding, K. Liu and W. Wang, *Appl. Phys. Lett.*, 2014, **104**, 173701.
23 Z. Li, Z. Huang, F. Sun, X. Li and J. Ma, *Mater. Today Adv.*, 2020, **7**, 100077.
24 J. Ma, X. Liang, X. Wu, Z. Liu and F. Gong, *Sci. Rep.*, 2015, **5**, 1–6.
25 J. Schroers, *Adv. Mater.*, 2010, **22**, 1566–1597.
26 H. Li, Z. Li, J. Yang, H. B. Ke, B. Sun, C. C. Yuan, J. Ma, J. Shen and W. H. Wang, *Sci. China Mater.*, 2021, **64**, 964–972.
27 S. N. Safri, M. T. Sultan, N. Saba and M. Jawaid, *Polym. Test.*, 2018, **71**, 362–369.
28 M. Fartini, M. Abdul Majid, M. Ridzuan, N. Amin and A. Gibson, *Plast., Rubber Compos.*, 2016, **45**, 136–146.
29 H. He, Z. Zhang, J. Wang and K. Li, *Composites, Part B*, 2013, **45**, 919–924.
30 J. Qiao, X. Zhang, C. Liu, L. Lyu, Z. Wang, L. Wu, W. Liu, F. Wang and J. Liu, *Composites, Part B*, 2020, **200**, 108343.
31 J. L. Chen, Z. Xu, S. B. Qu, X. Y. Wei and X. H. Liu, *Ceram. Int.*, 2008, **34**, 803–807.
32 P. S. Antonel, F. Berhó, G. Jorge and F. V. Molina, *Synth. Met.*, 2015, **199**, 292–302.
33 R. Zhang, P. Tang, J. Li, D. Xu and Y. Bin, *Polymer*, 2014, **55**, 2103–2112.
34 M. Dias, H. Mozetic, J. Barboza, R. Martins, L. Pelegrini and L. Schaeffer, *Powder Technol.*, 2013, **237**, 213–220.
35 X. Liang, L. Ling, C. Lu and L. Liu, *Mater. Lett.*, 2000, **43**, 144–147.
36 X. Li, X. Liang, Z. Zhang, J. Ma and J. Shen, *Scr. Mater.*, 2020, **185**, 100–104.
37 H. Tan, Z. Lu, H. Yao, B. Yao, Y. Feng and Y. Li, *Mater. Trans.*, 2001, **42**, 551–555.
38 A. Inoue, T. Nakamura, T. Sugita, T. Zhang and T. Masumoto, *Mater. Trans., JIM*, 1993, **34**, 351–358.
39 J. Tan, B. A. Sun, S. Scudino, K. G. Prashanth, W. W. Zhang, Y. Y. Li and J. Eckert, *Mater. Sci. Eng., A*, 2014, **600**, 53–58.
40 W. Chen, Z. Liu and J. Schroers, *Acta Mater.*, 2014, **62**, 49–57.
41 Z. Liu, W. Chen, J. Carstensen, J. Ketkaew, R. M. O. Mota, J. K. Guest and J. Schroers, *Acta Mater.*, 2016, **105**, 35–43.
42 N. Li, W. Chen and L. Liu, *JOM*, 2016, **68**, 1246–1261.
43 N. Stepanov, D. Shaysultanov, G. Salishchev, M. Tikhonovsky, E. Oleynik, A. Tortika and O. N. Senkov, *J. Alloys Compd.*, 2015, **628**, 170–185.
44 X. Li, D. Wei, J. Zhang, X. Liu, Z. Li, T. Wang, Q. He, Y. Wang, J. Ma and W. Wang, *Appl. Mater. Today*, 2020, **21**, 100866.

